

NANOSTRUCTURAL CHARACTERIZATION AND LATTICE STRAIN OF TiO₂-Al₂O₃-SiO₂ COATING ON GLASS AND SI (100) SUBSTRATES

M. RIAZIAN[†]

Department of Engineering, Tonekabon branch, Islamic Azad University, Tonekabon, Iran.

ABSTRACT

Synthesis of TiO₂-Al₂O₃-SiO₂ nanopowder composite, as well as composite coating on soda lime glass and Si (100) by sol-gel method is reported.

The morphology and the crystal structure of composite are characterized by the use of field emission scanning electron microscopy (FE-SEM), Energy dispersive X-ray (EDAX), atomic force microscopy (AFM) and X-ray diffraction (XRD) techniques. The effects of chemical compositions and Calcination temperature on surface topography and the crystallization of phases are studied. In addition, the lattice strain and coating roughness parameters are calculated during thermal treatment.

Keywords :Nanostructure; Lattice Strain; TiO₂-Al₂O₃-SiO₂; Composite; Coating; Sol-Gel method.

1. INTRODUCTION

TiO₂ powders and coatings are used as ceramic composites, and photo catalyst because of their special surface area and specula porosity¹. The photocatalytic performance of these compounds depends on the characteristic of the TiO₂ crystallites, such as the size and surface area. One of the applicable ways to vary the characteristics and property of TiO₂ crystallites is by importing a second semiconductor into the TiO₂ matrix. SiO₂ has been incorporated into the TiO₂ matrix to enhance the photocatalytic process²⁻⁴. Al₂O₃ and SiO₂ have high thermal stability, excellent mechanical strength and help to create new catalytic sites due to interaction between TiO₂ and SiO₂ also, SiO₂ acts as a carrier of TiO₂ and helps to obtain a large surface area as well as a suitable porous structure^{5, 6}. Due to their good resistance against alkaline solutions, Al₂O₃-TiO₂-SiO₂ coatings are attracting the attention of many scientists. Their alkaline resistance is strongly controlled by their surface state. It is well recognized that the properties of materials highly depend on size, morphology, and dimensionality⁷⁻¹², three crucial geometric parameters. TiO₂ can be synthesized by various techniques, such as precipitation¹³, chemical vapor deposition¹⁴, hydrothermal method¹⁵ and glycothermal method¹⁶.

In this work, TiO₂-Al₂O₃-SiO₂ composite is prepared by using the hydrolysis procedure of titanium tetraisopropoxide, tetraethoxysilane and aluminum tri-sec-butylate, which is transformed to anatase, Al₂O₃ and Al₂SiO₄ by heating it at 300, 600 and 900 °C. It obviously depends on the preparation procedures and TiO₂ precursor content in combination.

2. EXPERIMENTAL DETAILS

The composition of the starting solution and the experimental conditions used for ternary composite are listed in Table 1. The precursors, tetraethoxysilane (TEOS, Merck, ≥ 99%), titanium tetraisopropoxide (TTIP, (Ti(OPr)₄), Merck ≥ 98%), aluminum tri-sec-butylate (ATSB Merck, ≥ 97%), HCl (Merck, 36%, Ethanol (Merck ≥ 97%) and deionized water were used without further purification.

All the experimental processes were repeated for three times and all the data analysis were the same. The starting point of the fabrication was a solution prepared by mixing precursors in two different molar ratio (MR = 1 and MR = 2). (TEOS, deionized water, ethanol, HCl), (TTIP, deionized water, ethanol, HCl) and (ATSB, deionized water, ethanol, HCl) were dissolved separately at room temperature (RT) and stirred for 24 hours. After then, above solutions were mixed vigorously at RT. After 48 hours gelation was formed. The coatings were deposited on dried and clean soda lime glass slides and Si (100) substrates by spin coating at 4000 rpm. Mirror-polished n-type Si (100) samples were used as substrates. These substrates were cut into 3x1x0.2 cm³ and then slides were rinsed with ethanol in an ultrasonic bath. The coatings after dried in air were heated at 10 °C/min to 300 °C and held there for 2 hours. The gelation was heated at 50 °C for 24 hours to yield a powder. Finally, the obtained powders were calcined at three different temperatures, i.e.: 300, 600 and 900 °C.

Table 1. Composition of starting solutions and experimental conditions for ternary powders preparation.

Sol-gel Method used	Sol-gel Method step	Precursors and Molar ratio (MR)		Stirring Time (h)	PH
		TTIP/ ATSB/TEOS = 1:1/1.	TTIP/ ATSB/TEOS = 2:2/1.		
Alkoxide route	1	TEOS	TEOS/EtOH/HCl/H ₂ O = 1:50/0.1/2	24	2
		TIOT	TIOT/EtOH/HCl/H ₂ O = 1:50/0.1/2	24	5
		ATSB	ATSB/EtOH/HCl/H ₂ O = 1:50/0.1/2	24	3
	2	Mixing the precursors		48	3

XRD patterns were recorded on a GBC-MMA 007 (2000) X-ray diffractometer with Cu-Kα, 1.54056 Å, (0.02° step at 10°/min) radiation over a 2θ range of 10–80°. FE-SEM (S-4160 Hitachi) was used to investigate the morphology of the nanoparticles. For AFM (Easy Scan 2 Flex (Switzerland), measurements, the powder samples were first diluted in deionized water to the appropriate concentration (in a ratio of 1: 20 from a 0.04% aqueous suspension) and then ultrasonicated for 30 minutes. The 50 μl of the diluted solution was placed on a cleaned glass substrate (glass was cleaned with ethanol and acetone then dried with a nitrogen steam), incubated for 10 minutes, and then the residual solution was blown by a stream of nitrogen. The measurements were made at 20 °C and relative humidity of 45% using a silicon tip. FT-IR measurements performed on a 1730 Infrared Fourier Transform Spectrometer (Perkin-Elmer) using the potassium bromide as the background.

3. RESULTS AND DISCUSSION

Crystalline phases of the composite ceramic coatings were investigated by

using XRD (Figs. 1 and 2). Characteristics of the XRD peaks is summarized in Table 2. As shown in these figures, different crystalline phases are formed at different calcination temperatures. Amorphous structure are observed for the as-prepared, 300 and 600 °C samples due to short range ordering of network¹⁷⁻¹⁹ (Figs. 1 and 2), while, the sample observed at 900 °C showed a high degree of crystallinity. For nano-size materials, X-rays may be diffracted into a number of different directions and concluded in lower peak intensity. The peaks observed at 2θ values of anatase, Al₂SiO₅ and Al₂O₃ phases were compared with the standard powder diffraction card of Crystal impact AMCS (99-101-0957), (99-100-4107) and (99-200-0017) respectively. The grain size was calculated from Scherrer's equation, $r = \frac{k\lambda}{2\beta \cos \theta}$, where β is FWHM

(full width at half maximum) observed, shape factor k is assumed to be 0.9 and λ is a wavelength of Cu-Kα radiation (0.154056 nm).

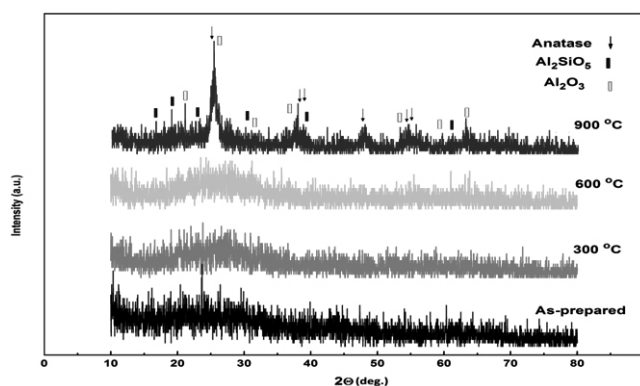


Figure 1. XRD patterns of $\text{TiO}_2\text{-Al}_2\text{O}_3\text{-SiO}_2$ for molar ratio (MR = 1) obtained from: without hydrothermal treatment (as-prepared), calcined at 300 °C, calcined at 600 °C and calcined at 900 °C.

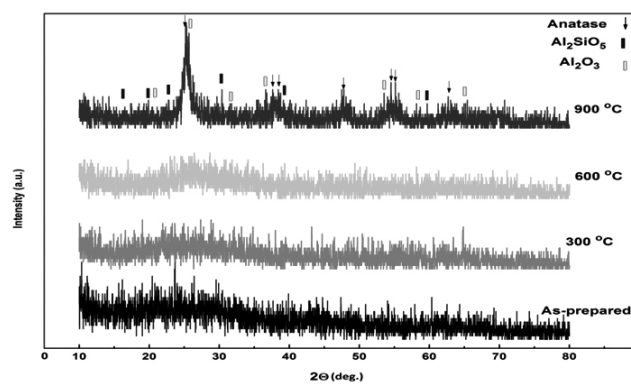


Figure 2. XRD patterns of $\text{TiO}_2\text{-Al}_2\text{O}_3\text{-SiO}_2$ for molar ratio (MR = 2) obtained from: without hydrothermal treatment (as-prepared), calcined at 300 °C, calcined at 600 °C and calcined at 900 °C.

Table 2. The 2θ angle, d-space, Miller indexes, grain size of $\text{TiO}_2\text{-Al}_2\text{O}_3\text{-SiO}_2$.

Molar ratio TTIP/ATSB/TEOS = 1:1/1. calcined at 900 °C			
Phase	2θ	d-space(A°)	size(nm)
Anatase Tetragonal a=3.8040 Å c=9.6140 Å	25.20	3.52	32
Al_2O_3 Hexagonal a=4.8440 Å c=13.2700 Å	25.80	3.46	25
Al_2SiO_5 Orthorhombic a=7.4839 Å b=7.6726 Å c=5.7681 Å	26.39	3.39	7
Molar ratio TTIP/ATSB/TEOS = 2:2/1 calcined at 900 °C			
Phase	2θ	d-space(A°)	size(nm)
Anatase Tetragonal a=3.8040 Å c=9.6140 Å	25.30	3.51	25
Al_2O_3 Hexagonal a=4.8440 Å c=13.2700 Å	25.90	3.45	12
Al_2SiO_5 Orthorhombic a=7.4839 Å b=7.6726 Å c=5.7681 Å	26.40	3.36	6

The influence of molar ratio on grain size of different phases, as seen by the decrease in size of grains when the molar ratio is increased due to the increase in the content of TTIP and ATSB in composite (Table 2). Since the atomic radii of Si atom is smaller than Ti, the TiO_2 particle experiences a contraction and its crystalline grows is retarded due to the Si atom. However, high composition of SiO_2 component leads to the formation of larger second particles of TiO_2 . This is due to the SiO_2 which behaves as a “neck” and connects the TiO_2 particles^{20,21}

Lattice strain (ϵ) of nanocrystallites were determined for dependence of FWHM on diffraction lines observed in 2θ range of 10-80° on $\sin \theta$ according to Williamson-Hall's equation²², $\beta \cos \theta = \frac{k\lambda}{L} + 4\epsilon \sin \theta$ where β is FWHM, shape factor k is assumed to be 0.9 similar to Scherrer equation. λ (wavelength of Cu-K α).

Lattice strain was determined from the slope of the linear plots of $\beta \cos \theta$

against $4\sin \theta$. Due to poorly crystallized powder samples, the linearity between $\beta \cos \theta$ and $4\sin \theta$ is not very good²³. The plots of $\beta \cos \theta$ against $4\sin \theta$ for different diffraction lines are illustrated in Fig. 3. For low calcination temperatures, experimental points for diffraction lines are scattered because the peaks are weak and broad, therefore, their FWHMs are difficult to measure. It can be seen that lattice strain decreases from 0.482 to 0.197 by increasing the molar ratio. By increasing the molar ratio, the content of SiO_2 and the porosity in composite decreases and the lattice possesses a more arrangement.

The FE-SEM images of $\text{TiO}_2\text{-Al}_2\text{O}_3\text{-SiO}_2$ nanoparticles are shown in Figs. 4-7. In Figs. 4 and 5, it is clear that by increasing the molar ratio and content of TiO_2 and Al_2O_3 , the aggregation of particles becomes larger. The shapes of the particles are similar to each other and likely to become spherical at the 900 °C calcination temperature and as-prepared state. As shown in Figs. 6 and 7,

for more TiO_2 and Al_2O_3 concentration (higher molar ratio) and higher calcination temperatures, the coating samples show more particle compression and fewer pores. The FE-SEM images of coatings with MR = 1 have smooth surface and very low particle compression. It can be indicated that silicon substrates have more adhesion to composite than glass substrates, because of the silicon substrate have more dangling bonds therefore, SiO_2 content in composite react with them

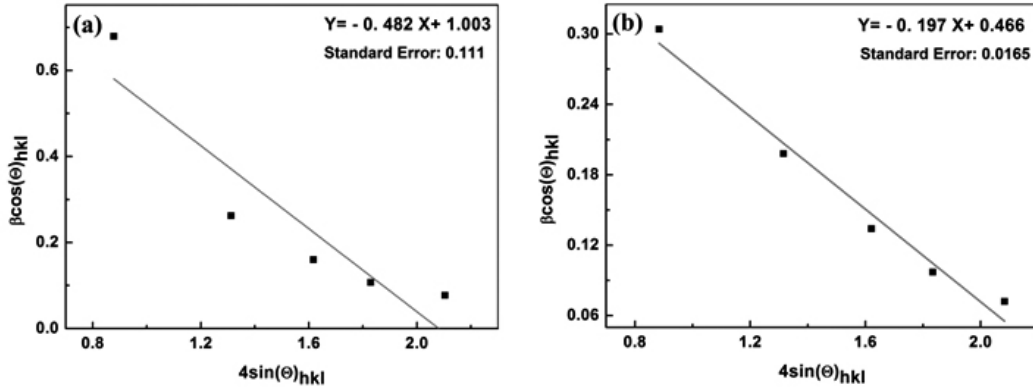


Figure 3. Relation between $\beta \cos \theta$ and $4 \sin \theta$ (Williamson-Hall plots) at 900 °C calcined temperature (a) for MR = 1, (b) for MR = 2.

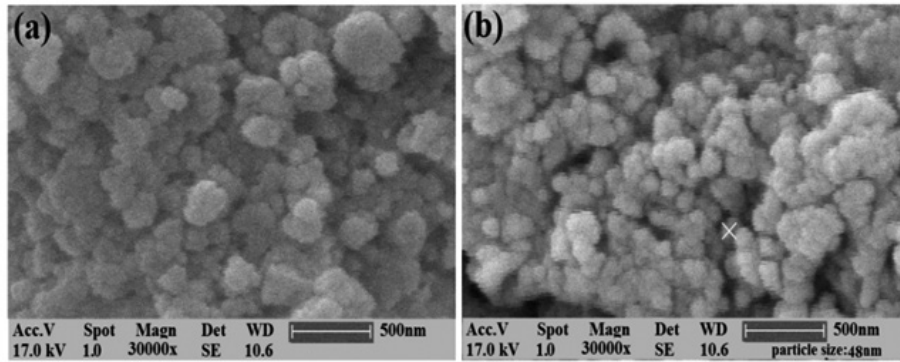


Figure 4. SEM images of $\text{TiO}_2\text{-Al}_2\text{O}_3\text{-SiO}_2$ as-prepared powder (a) MR = 1, (b) MR = 2.

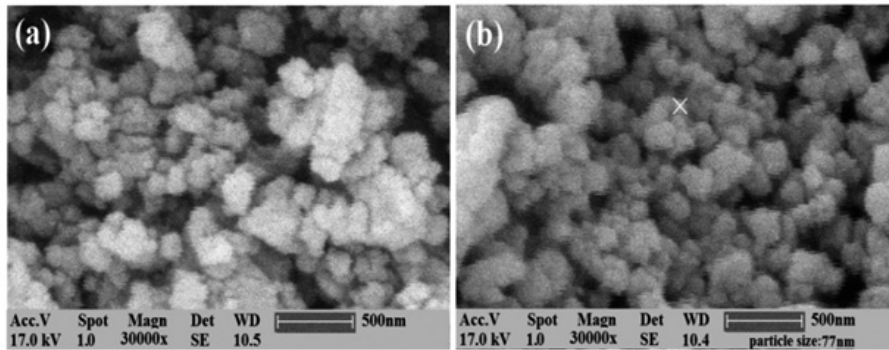


Figure 5. SEM images of $\text{TiO}_2\text{-Al}_2\text{O}_3\text{-SiO}_2$ powder calcined at 900 °C (a) MR = 1, (b) MR = 2.

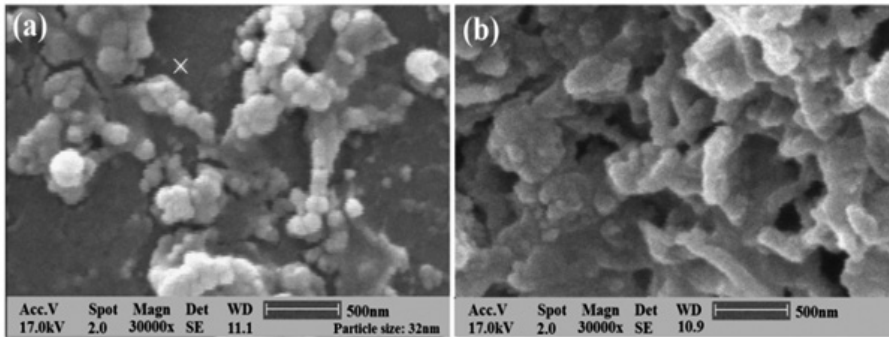


Figure 6. SEM images of $\text{TiO}_2\text{-Al}_2\text{O}_3\text{-SiO}_2$ coating on Si (100) substrate calcined at 300 °C (a) MR = 1, (b) MR = 2.

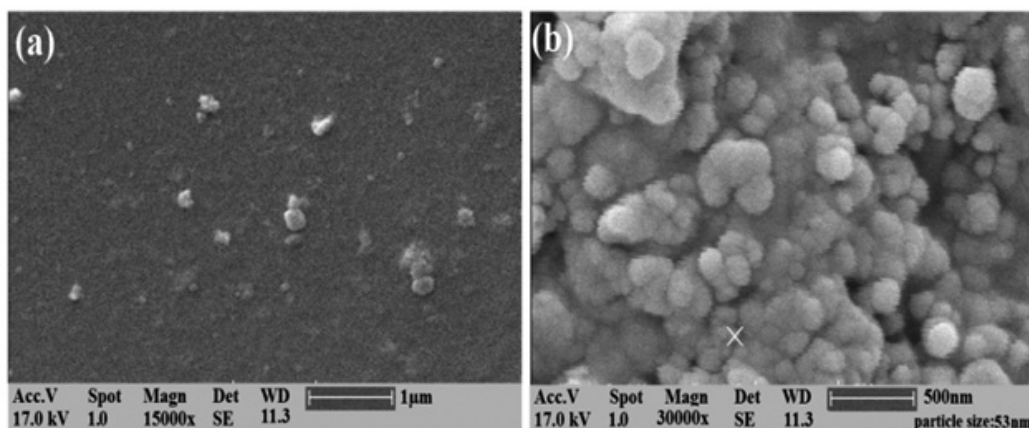


Figure 7. SEM images of $\text{TiO}_2\text{-Al}_2\text{O}_3\text{-SiO}_2$ coating on glass substrate calcined at $300\text{ }^\circ\text{C}$ (a) $\text{MR} = 1$, (b) $\text{MR} = 2$.

The presence of the participants in two different molar ratios for powders and coatings according to Table 1., are confirmed by EDAX spectra (Fig. 8). As can be seen in Table 3., the results indicate the presence of TiO_2 , Al_2O_3 and SiO_2 in the powder and coating samples.

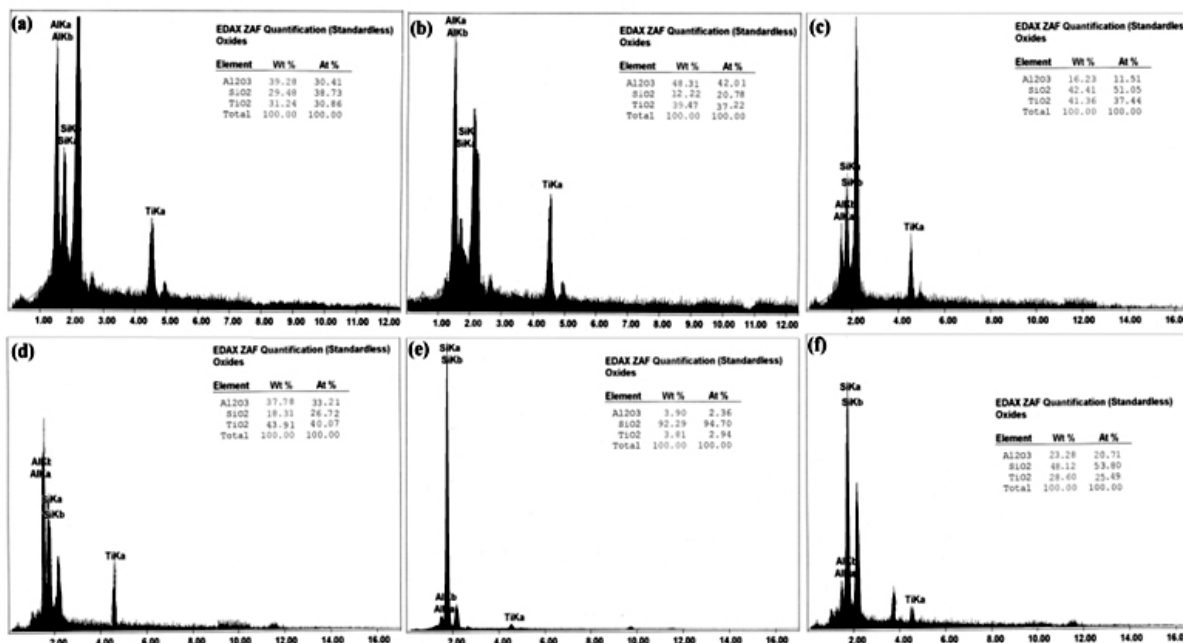


Figure 8. EDX results for powder composite (a) $\text{MR} = 1$ and (b) $\text{MR} = 2$ sample, for coating composite on Si (100) (c) $\text{MR} = 1$ and (d) $\text{MR} = 2$, for coating composite on glass (e) $\text{MR} = 1$ and (f) $\text{MR} = 2$.

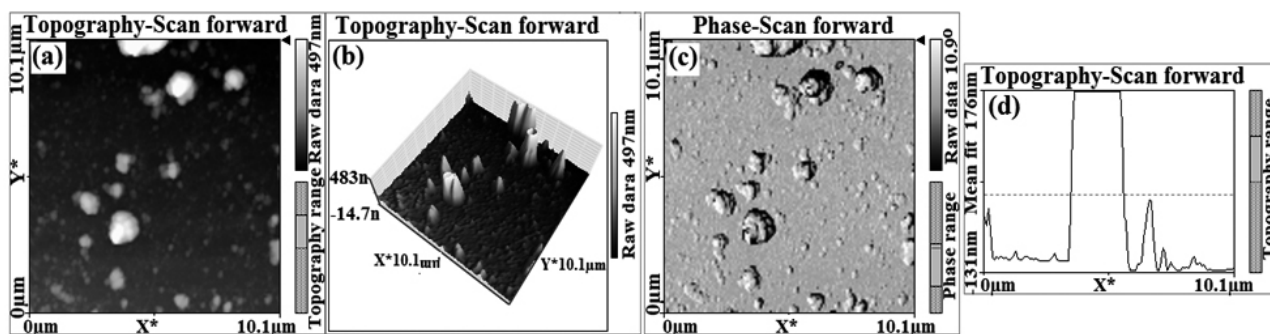


Figure 9. AFM images of $\text{TiO}_2\text{-Al}_2\text{O}_3\text{-SiO}_2$ powder in as-prepared state in $\text{MR} = 1$, (a) topography-scan forward, (b) topography-3D scan forward, (c) phase-scan forward and (d) roughness and topography-scan forward.

Table 3. Chemical composition obtained from EDX.

Oxide	Weight percent	Atomic percent	Error (%)
Molar ratio TIOT/ATSB/ TEOS =1 Powder sample			
Al ₂ O ₃	39.28	30.41	1.59
SiO ₂	29.48	38.73	2.17
TiO ₂	31.24	30.86	2.46
Molar ratio TIOT/ATSB/ TEOS =2 Powder sample			
Al ₂ O ₃	48.31	42.01	2.25
SiO ₂	12.22	20.78	3.16
TiO ₂	39.47	37.22	2.51
Molar ratio TIOT/ATSB/ TEOS =1 Coating on Si (100)			
Al ₂ O ₃	16.23	11.51	2.16
SiO ₂	42.41	51.05	5.40
TiO ₂	41.36	37.44	5.30
Molar ratio TIOT/ATSB/ TEOS =2 Coating on Si (100)			
Al ₂ O ₃	37.78	33.21	1.73
SiO ₂	18.31	26.72	4.27
TiO ₂	43.91	40.07	3.18
Molar ratio TIOT/ATSB/ TEOS =1 Coating on glass			
Al ₂ O ₃	3.90	2.36	2.78
SiO ₂	92.29	94.70	0.55
TiO ₂	3.81	2.94	4.16
Molar ratio TIOT /ATSB/ TEOS =2 Coating on glass			
Al ₂ O ₃	23.28	20.71	1.43
SiO ₂	48.12	53.80	2.32
TiO ₂	28.60	25.49	2.87

The surface morphology of TiO₂-Al₂O₃-SiO₂ coating and powder nanoparticles are shown in Figs. 9-16. The AFM images show the representative 3-D and phase scan surface morphologies of the composite powders and coatings. Figs. 9-12 show the surface morphology of TiO₂-Al₂O₃-SiO₂ powder

with the molar ratio of 1 and 2 calcined at as-prepared and 900 °C calcination temperature respectively. Figs. 13-16 show the surface morphology of the coating on glass and Si (100) substrates with the molar ratio of 1 and 2 calcined at 300 °C respectively.

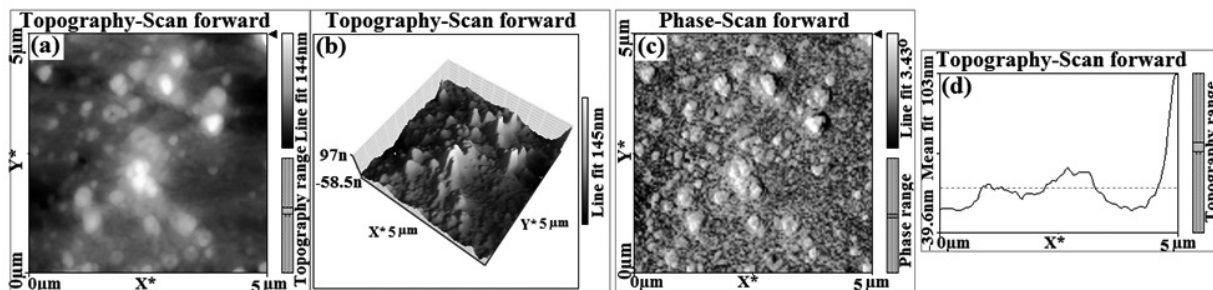


Figure 10. AFM images of TiO₂-Al₂O₃-SiO₂ powder in as-prepared state and MR = 2, (a) topography-scan forward, (b) topography-3D scan forward, (c) phase-scan forward and (d) roughness and topography-scan forward.

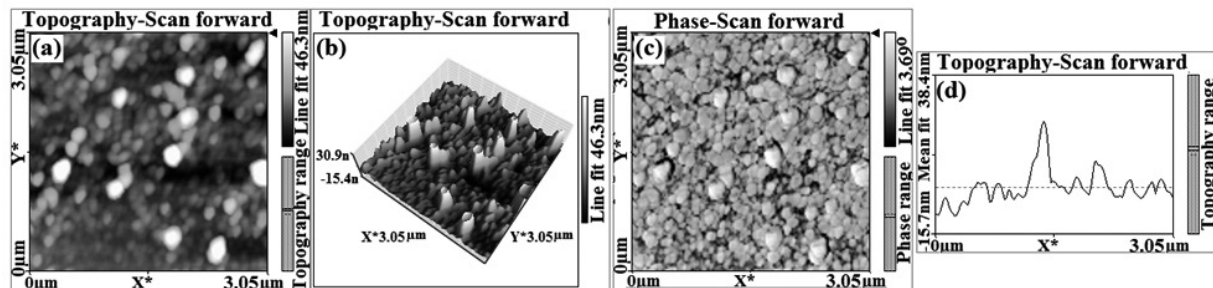


Figure 11. AFM images of TiO₂-Al₂O₃-SiO₂ powder at 900 °C calcined temperature and MR = 1, (a) topography-scan forward, (b) topography-3D scan forward, (c) phase-scan forward and (d) roughness and topography-scan forward.

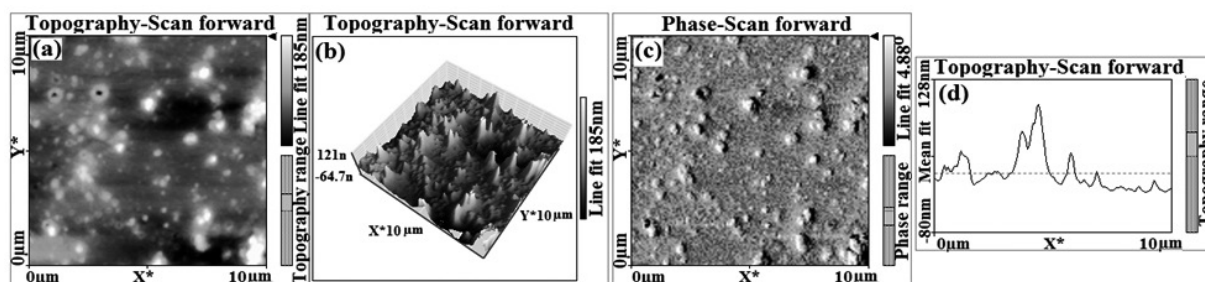


Figure 12. AFM images of $\text{TiO}_2\text{-Al}_2\text{O}_3\text{-SiO}_2$ powder at 900 °C calcined temperature and MR = 2, (a) topography-scan forward, (b) topography-3D scan forward, (c) phase-scan forward and (d) roughness and topography-scan forward.

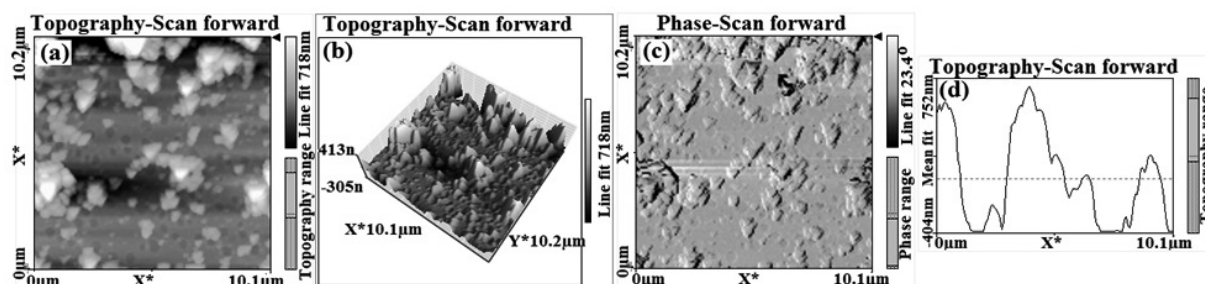


Figure 13. AFM images of $\text{TiO}_2\text{-Al}_2\text{O}_3\text{-SiO}_2$ coating on Si (100) substrate calcined at 300 °C and MR = 1, (a) topography-scan forward, (b) topography-3D scan forward, (c) phase-scan forward and (d) roughness and topography-scan forward.

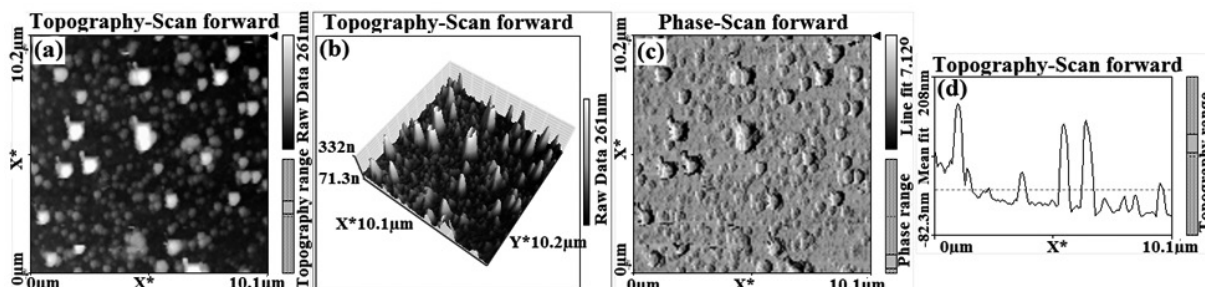


Figure 14. AFM images of $\text{TiO}_2\text{-Al}_2\text{O}_3\text{-SiO}_2$ coating on Si (100) substrate calcined at 300 °C and MR = 2, (a) topography-scan forward, (b) topography-3D scan forward, (c) phase-scan forward and (d) roughness and topography-scan forward.

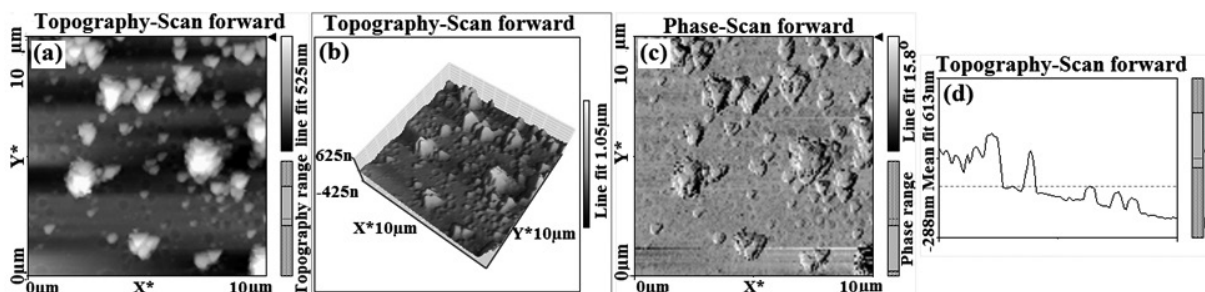


Figure 15. AFM images of $\text{TiO}_2\text{-Al}_2\text{O}_3\text{-SiO}_2$ coating on glass substrate calcined at 300 °C and MR = 1, (a) topography-scan forward, (b) topography-3D scan forward, (c) phase-scan forward and (d) roughness and topography-scan forward.

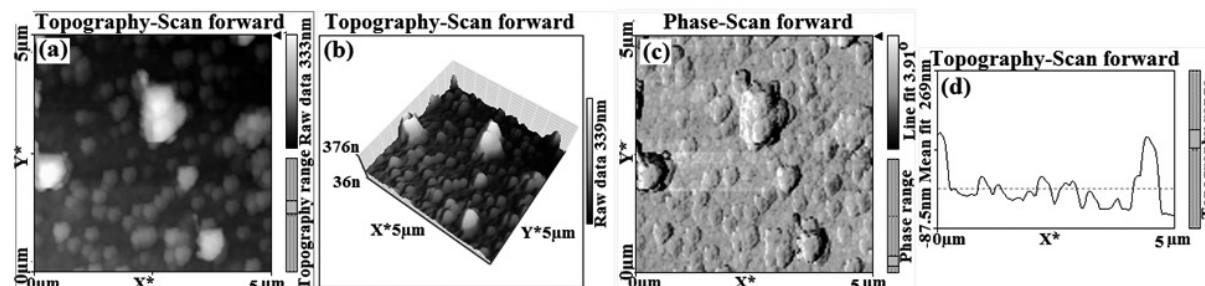


Figure 16. AFM images of $\text{TiO}_2\text{-Al}_2\text{O}_3\text{-SiO}_2$ coating on glass substrate calcined at 300 °C and MR = 2, (a) topography-scan forward, (b) topography-3D scan forward, (c) phase-scan forward and (d) roughness and topography-scan forward.

The surface morphologies are characterized by average thickness of the sheets, intervals between the sheet and the roughness parameters such as S_a , S_m and S_q shown in Table 4. The parameter S_a is the roughness average given by $S_a = \frac{1}{N} \sum_{i=0}^{N-1} |Z(x_i)|$. Moreover, S_m is the mean value given by $S_m = \frac{1}{N} \sum_{i=0}^{N-1} Z(x_i)$ and the parameter S_q is the root mean square given by $S_q = \sqrt{\frac{1}{N} \sum_{i=0}^{N-1} Z(x_i)^2}$.

Table 4. Roughness parameter of TiO₂-Al₂O₃-SiO₂ powder and coating samples.
Roughness parameter of the TiO₂-Al₂O₃-SiO₂ powder samples

Sample	S _a (nm)	Err (%)	S _q (nm)	Err (%)	S _m (pm)	Err (%)
MR=1 as-prepared	16.03	0.51	22.12	1.07	45.84	1.75
MR=2 as-prepared	78.50	1.01	109.98	2.91	78.30	2.37
MR=1 calcined at 900 °C	5.65	0.21	8.89	0.31	46.06	1.57
MR=2 calcined at 900 °C	21.00	0.55	31.28	0.21	46.10	1.06
Roughness parameter of the TiO ₂ -Al ₂ O ₃ -SiO ₂ coating samples						
MR=2 Coating of SiO ₂ on glass	26.44	0.78	35.28	0.82	43.42	0.61
MR=2 Coating of Al ₂ O ₃ on glass	130.85	3.07	200.41	1.66	36.77	1.57
MR=2 Coating of TiO ₂ on glass	207.86	2.34	259.90	2.77	21.65	0.92
MR=1 TiO ₂ -Al ₂ O ₃ -SiO ₂ coating on glass	68.34	1.82	102.57	1.37	37.35	1.42
MR=2 TiO ₂ -Al ₂ O ₃ -SiO ₂ coating on glass	124.94	1.92	136.63	2.02	124.94	2.33
MR=1 TiO ₂ -Al ₂ O ₃ -SiO ₂ coating on Si(100)	87.28	1.31	132.35	0.81	44.24	1.39
MR=2 TiO ₂ -Al ₂ O ₃ -SiO ₂ coating on Si(100)	130.43	1.78	138.87	2.01	130.43	1.80

By Comparison of Figs. 9-16 and Table 3, roughness of the composite powder and coatings surface increases by increasing the content of TiO₂ and Al₂O₃ precursors in molar ratio, therefore the roughness of samples with MR = 2 seems to become greater than of samples with MR = 1. The higher of TiO₂ and Al₂O₃ content is, the more quickly the hydrolysis and condensation polymerization proceeds, which leads to higher viscosity of the solution²⁴. It should be responsible for the higher roughness. Although by increasing the calcination temperature, the roughness becomes smaller than as-prepared state. Calcination temperature smoothes the surface due to it is responsible for rearranging the particles to have lowest free energy and minimum stress.

The FTIR spectra of TiO₂-Al₂O₃-SiO₂ powder calcined at different temperatures are shown in Fig. 17. The composite of each sample shows the fundamental vibration modes. In the as-prepared gel, the 3200 cm⁻¹ band is

attributed to hydroxyl groups from water and ethanol occluded in the titania pore. Besides, the OH bending band of water in gel is observed at 1650 cm⁻¹ and low energy interval Ti-O band are found at 1061 and below 1000 cm⁻¹. The IR spectra show characteristic peaks of molecular water (1621 cm⁻¹), Ti-O (653–550 cm⁻¹), Al-O (780, 570 cm⁻¹) and Si-O (1050,450 cm⁻¹). However, the absorption peak at 1090 cm⁻¹ and 1010 cm⁻¹ indicate the Si-O-Si linkage in the composite. The absorption peak of Si-O-Ti linkage is observed at 925 cm⁻¹. Therefore, the formation of Al-O-Ti and Al-O-Si (or Al-O-Ti-O-Si) bonds is possible. In dye-sensitized solar cells, fictionalization of TiO₂ thin coatings with siloxane adsorbates has been shown to be useful as a surface passivation technique that hinders the recombination processes and improves the overall efficiency of light-to-electricity conversion²⁵.

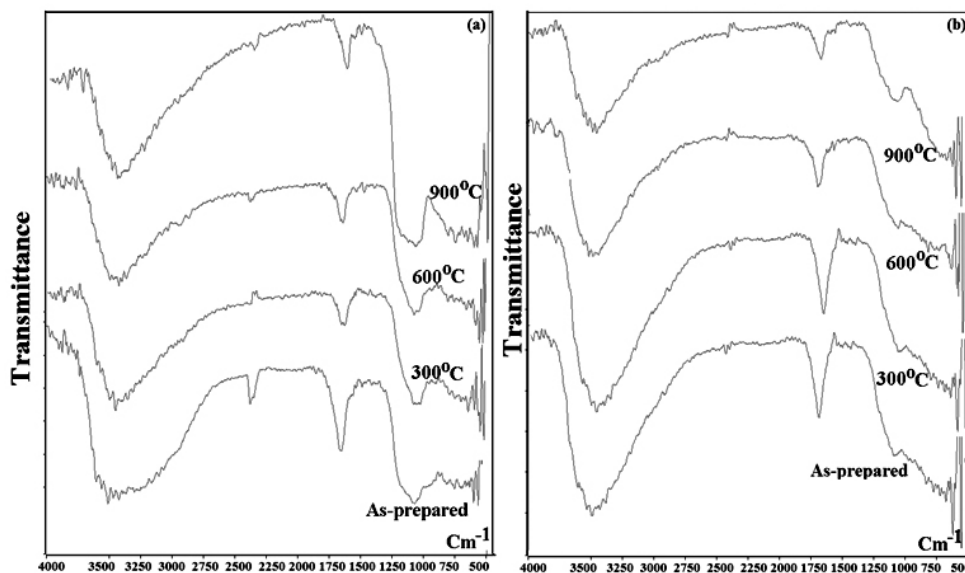


Figure 17. FTIR spectra of TiO₂-Al₂O₃-SiO₂ composite calcined at different temperature.

4. CONCLUSIONS

The present study shows that, homogeneous hydrolysis of a metal alkoxide provides an excellent technique for preparation of nanoparticle materials. The results indicated that homogeneous hydrolysis of titanium tetraisopropoxide and aluminum tri-sec-butylate via sol-gel route is a promising technique for preparing photosensitive material with uniform nanoparticles. In this study, nanocrystalline $\text{TiO}_2\text{-Al}_2\text{O}_3\text{-SiO}_2$ particles have been successfully synthesized by chemical method and heat treatment process. The influence of calcination temperatures and molar ratio of precursors can affect structural and morphological properties such as size, strain and roughness. Average crystallite size increases with an increase in calcination temperatures.

ACKNOWLEDGMENT

Special thanks to Islamic Azad University, Tonekabon branch for their financial support.

REFERENCES

1. M. Riazian, *J. Nanostructures*, 4, 433, (2014).
2. M. V. Roldan, Y. Castro, N. Pellegrini, A. Duran, *J. Sol-Gel Sci. Technol.* 76, 180, (2015).
3. F. Zhang, D. Sun, C. Yu, Y. Yin, H. Dai, G. Shao, *New J. Chem.* 39, 3065, (2015).
4. J. Hegmann, R. Jahn, S. Schonau, N. Sommer, P. Lobmann, *J. Sol-Gel Sci. Technol.* 74, 585, (2015).
5. A. B. Isaev, F. F. Orudjevedova, F. G. Gasanova, I. Kh. Hkizrieva, *Nanotechnologies in Russia*. 10, 357, (2015).
6. M. Gao, L. Zhu, W. L. Ong, J. Wang, G. W. Ho, *Catal. Sci. Tech.* 5, 4703, (2015).
7. M. Riazian, *Indian J. Chem. A*, 53, 1377, (2014).
8. M. Riazian, A. Bahari, *Pramana J. Phys.* 78, 319, (2012).
9. M. Riazian, A. Bahari, *Inter. J. Phys. Sci.* 6, 3604, (2011).
10. M. Riazian, *J. Korean Phys. Soc.* 62, 459, (2013).
11. M. Riazian, *Indian J. Phys.* 87, 991, (2013).
12. A. Y. Arasi, J. J. Latha, B. Sundaresan, V. Dhanalakshmi, R. Anbarasan, *J. Chilean Chem. Soc.* 56, 635, (2011).
13. A. D. Paola, G. Cufalo, M. Addamo, M. Bellardita, R. Campostrini, M. Ischia, R. Ceccato, L. Palmisano, *Colloids and Surfaces A: Physicochem. Eng. Aspects*, 317, 366, (2008).
14. Z. Ding, X. J. Hu, G. Q. Lu., P. L. Yue, P. F. Greenfield, *Langmuir*, 16, 6216, (2000).
15. J. Yang, S. Mei, *J. American Ceramic Soc.* 8, 1696 (2001).
16. S. Iwamoto, W. Tanakulrungsank, M. Inoue, K. Kagawa, P. Praserttham, *J. Mat. Sci. Lett.* 19, 1439, (2001).
17. J. Qiu, et al. *J. Mater. Chem.* 22, 3549, (2012).
18. S. R. Gajjala, K. Ananthanarayanan, C. Yap, M. Grätzel, P. Balaya, *Energy Environ. Sci.* 3, 838, (2010).
19. Q. Li., et al. *Mate. Sci.* 900, 1823, (2012).
20. L. Zhou, S. Yan, B. Tian, J. Zhang, M. Anpo, *Material Lett.* 60, 396, (2006).
21. L. A. O'Dell, S. L. P. Savin, A. V. Chadwick, M. E. Smith, *J. Phys. Chem. C*. 111, 13740, (2007).
22. A. K. Zaka, W. H. Abd. Majida, M. E. Abrishamib, R. Yousefi, *Solid State Sci.* 13, 251, (2011).
23. M. Inagaki, R. Nonaka, B. Tryba, A. W. Morawski, *Chemosphere*. 64, 437, (2006).
24. Y. Du, G. H. Frischat, *J. Mat. Sci.* 35, 2561, (2000).
25. N. Iguchi, C. Cady, R. C. Snoberger, B. M. Hunter, E. M. Sproviero, C. A. Schmuttenmaer, R. H. Crabtree, G. W. Brudvig, V. S. Batista, *Characterization of siloxane adsorbates covalently attached to TiO_2* , Proc. SPIE, 7034, (2008), *Physical Chemistry of Interfaces and Nanomaterials VII*, San Diego, California, USA.